

## Dislocations in AlGa<sub>N</sub>: core structure, atom segregation and optical properties

Fabien C-P. Massabuau, Sneha L. Rhode, Matthew K. Horton, Thomas J. O'Hanlon, Andras Kovacs, Marcin S. Zielinski, Menno J. Kappers, Rafal E. Dunin-Borkowski, Colin J. Humphreys, and Rachel A. Oliver

*Nano Lett.*, **Just Accepted Manuscript** • DOI: 10.1021/acs.nanolett.7b01697 • Publication Date (Web): 14 Jul 2017

Downloaded from <http://pubs.acs.org> on July 14, 2017

### Just Accepted

"Just Accepted" manuscripts have been peer-reviewed and accepted for publication. They are posted online prior to technical editing, formatting for publication and author proofing. The American Chemical Society provides "Just Accepted" as a free service to the research community to expedite the dissemination of scientific material as soon as possible after acceptance. "Just Accepted" manuscripts appear in full in PDF format accompanied by an HTML abstract. "Just Accepted" manuscripts have been fully peer reviewed, but should not be considered the official version of record. They are accessible to all readers and citable by the Digital Object Identifier (DOI®). "Just Accepted" is an optional service offered to authors. Therefore, the "Just Accepted" Web site may not include all articles that will be published in the journal. After a manuscript is technically edited and formatted, it will be removed from the "Just Accepted" Web site and published as an ASAP article. Note that technical editing may introduce minor changes to the manuscript text and/or graphics which could affect content, and all legal disclaimers and ethical guidelines that apply to the journal pertain. ACS cannot be held responsible for errors or consequences arising from the use of information contained in these "Just Accepted" manuscripts.

# Dislocations in AlGa<sub>0.46</sub>N: core structure, atom segregation and optical properties

*Fabien C-P. Massabuau*<sup>\*1</sup>, *Sneha L. Rhode*<sup>2</sup>, *Matthew K. Horton*<sup>3</sup>, *Thomas J. O'Hanlon*<sup>1</sup>,  
*András Kovács*<sup>4</sup>, *Marcin S. Zielinski*<sup>5</sup>, *Menno J. Kappers*<sup>1</sup>, *Rafal E. Dunin-Borkowski*<sup>4</sup>, *Colin J.*  
*Humphreys*<sup>1</sup>, and *Rachel A. Oliver*<sup>1</sup>

<sup>1</sup> Department of Materials Science and Metallurgy, University of Cambridge, Cambridge CB3  
0FS, UK

<sup>2</sup> Department of Materials, Imperial College London, London SW7 2AZ, UK

<sup>3</sup> Materials Science and Engineering, University of California Berkeley, Berkeley, CA 94720,  
US

<sup>4</sup> Ernst Ruska-Centre for Microscopy and Spectroscopy with Electrons and Peter Grünberg  
Institute, Forschungszentrum Jülich GmbH, D-52425 Jülich, Germany

<sup>5</sup> Attolight AG, EPFL Innovation Park, 1015 Lausanne, Switzerland

## Abstract

We conducted a comprehensive investigation of dislocations in Al<sub>0.46</sub>Ga<sub>0.54</sub>N. Using aberration-corrected scanning transmission electron microscopy and energy dispersive X-ray spectroscopy,

1  
2  
3 the atomic structure and atom distribution at the dislocation core have been examined. We report  
4  
5 that the core configuration of dislocations in AlGa<sub>N</sub> is consistent with that of other materials in  
6  
7 the III-Nitride system. However we observed that the dissociation of mixed-type dislocations is  
8  
9 impeded by alloying GaN with AlN, which is confirmed by our experimental observation of Ga  
10  
11 and Al atom segregation in the tensile and compressive parts of the dislocations, respectively.  
12  
13 Investigation of the optical properties of the dislocations shows that the atom segregation at  
14  
15 dislocations has no significant effect on the intensity recorded by cathodoluminescence in the  
16  
17 vicinity of the dislocations. These results are in contrast with the case of dislocations in  
18  
19 In<sub>0.09</sub>Ga<sub>0.91</sub>N where segregation of In and Ga atoms also occurs but results in carrier localization  
20  
21 limiting non-radiative recombination at the dislocation. This study therefore sheds light on why  
22  
23 InGa<sub>N</sub>-based devices are generally more resilient to dislocations than their AlGa<sub>N</sub>-based  
24  
25 counterparts.  
26  
27  
28  
29  
30  
31  
32

### 33 **Keywords**

34  
35 AlGa<sub>N</sub>, InGa<sub>N</sub>, dislocation, aberration-corrected TEM, cathodoluminescence.  
36  
37  
38  
39  
40  
41  
42  
43

44 The III-Nitride system is a very important family of semiconducting materials for light  
45  
46 emitting diode (LED) technology. The development of GaN opened the path for efficient LEDs<sup>1</sup>.  
47  
48 While alloying GaN with InN addresses the question of light emission in the visible spectrum<sup>2</sup>,  
49  
50 alloying with AlN paves the way for applications enabled by ultra-violet (UV) light such as  
51  
52 water disinfection, skin condition phototherapy, and forensic identification among others<sup>3</sup>.  
53  
54 However, the performance of III-Nitride LEDs varies substantially with the emission  
55  
56  
57  
58  
59  
60

1  
2  
3 wavelength. Whilst external quantum efficiencies of 84% and 44% can be achieved for blue<sup>4</sup> and  
4  
5 green<sup>5</sup> LEDs, respectively, that of UV LEDs still remains under 10%<sup>3</sup>. While InGaN-based  
6  
7 devices exhibit a remarkable resilience to high densities of dislocations<sup>6</sup>, dislocations are thought  
8  
9 to be a significant factor limiting the efficiency of AlGaN-based LEDs<sup>7</sup>. It is therefore important  
10  
11 to understand the properties of dislocations in AlGaN and how these may differ from InGaN.  
12  
13

14  
15 Dislocations in III-Nitrides fall into three categories depending on their Burgers vector **b**, that  
16  
17 is, edge-type (**b** = **a**), mixed-type (**b** = **a** + **c**) and screw-type (**b** = **c**) dislocations<sup>8</sup>. The atomic  
18  
19 structure of the dislocation core in GaN and InGaN has been the subject of numerous  
20  
21 experimental<sup>9-14</sup> and theoretical<sup>15-21</sup> investigations because of its potential influence on the  
22  
23 formation of mid-gap states which can act as non-radiative recombination centers. In comparison  
24  
25 very little is known about dislocations in AlGaN, and their atomic structure has not been yet  
26  
27 reported. The present work aims to conduct a comprehensive study of dislocations in AlGaN. We  
28  
29 thus conducted a statistically meaningful observation of the core structure, of compositional  
30  
31 variations, and of the optical behavior of dislocations in AlGaN. To fully grasp the different  
32  
33 impact dislocations may have in AlGaN and InGaN alloys, the same analysis was conducted on  
34  
35 dislocations in InGaN.  
36  
37  
38  
39

40  
41 AlGaN and InGaN epilayers were grown by metal-organic vapor phase epitaxy (MOVPE) in a  
42  
43 Thomas Swan 6 x 2 inch close-coupled showerhead reactor. Trimethylgallium (TMG),  
44  
45 trimethylaluminium (TMA), trimethylindium (TMI), diluted silane in hydrogen (SiH<sub>4</sub>) and  
46  
47 ammonia (NH<sub>3</sub>) were used as precursors for the Ga, Al, In, Si and N elements, respectively.  
48  
49 Hydrogen (H<sub>2</sub>) was used as carrier gas for the growth of GaN, AlN and AlGaN, while a mixture  
50  
51 of hydrogen and nitrogen (N<sub>2</sub>) was employed for the growth of InGaN.  
52  
53  
54  
55  
56  
57  
58  
59  
60

1  
2  
3 For the AlGa<sub>x</sub>N epilayer, a *c*-plane sapphire substrate was employed. Following the growth of a  
4 30 nm AlN buffer layer at 1050 °C, a 2 μm AlN layer was grown at 1130 °C. A SiN<sub>x</sub> interlayer  
5 was then deposited to allow for the subsequent growth of faceted GaN islands at 980 °C for 120  
6 s. Finally the 3 μm Al<sub>x</sub>Ga<sub>1-x</sub>N epilayer with an Al content of  $x \sim 46\%$  was deposited at 1090 °C.  
7 X-ray diffraction on a Philips X'Pert MRD diffractometer was used to determine the composition  
8 and strain state of the layer. From reciprocal space maps taken on the 004 and 105 reflections,  
9 the AlGa<sub>x</sub>N layer was found to be 89% relaxed with regard to the strain-free AlN layer. Further  
10 details about the growth of the sample can be found in Ref. 22.  
11  
12  
13  
14  
15  
16  
17  
18  
19  
20  
21

22 For the InGa<sub>x</sub>N epilayer, a *c*-plane sapphire substrate was employed. A 5 μm GaN buffer layer  
23 (of which 2 μm undoped and 3 μm Si-doped to  $5 \times 10^{18} \text{ cm}^{-3}$ ) was then deposited. Following the  
24 growth of an additional 500 nm of GaN, a 135 nm In<sub>x</sub>Ga<sub>1-x</sub>N epilayer with an In content of  $x \sim$   
25 9% was deposited at 749 °C. (This particular composition of InGa<sub>x</sub>N was chosen because it has  
26 been thoroughly studied previously<sup>23</sup>.) From reciprocal space maps taken on the 006 and 204  
27 reflections, the InGa<sub>x</sub>N layer was found to be fully strained to the GaN pseudo-substrate. Further  
28 details about the growth of the sample can be found in Ref. 23.  
29  
30  
31  
32  
33  
34  
35  
36  
37  
38

39 Dislocations in the AlGa<sub>x</sub>N epilayer were observed by aberration-corrected high-angle annular  
40 dark field scanning transmission electron microscopy (HAADF-STEM) using an FEI Titan G2  
41 80-200 ChemiSTEM<sup>24</sup> and FEI Titan G3 50-300 PICO<sup>25</sup> microscopes operating at 300 kV with a  
42 detector collection semi-angle of 69 mrad. The sample was prepared for plan-view TEM imaging  
43 using standard mechanical polishing method followed by Ar<sup>+</sup> ion milling at 5 kV and cleaning  
44 from 1 kV down to 0.1 kV. The dislocations were viewed end-on - *i.e.* along the [0001] zone-  
45 axis - therefore allowing for the identification of the core structure<sup>9-12</sup>. Eshelby Twist, which is  
46 an apparent rotation of the lattice caused by the relaxation of stresses at the free surface caused  
47  
48  
49  
50  
51  
52  
53  
54  
55  
56  
57  
58  
59  
60

1  
2  
3 by the screw component of a dislocation<sup>26</sup>, was observed for all mixed-type dislocations. Focal  
4 series images for all dislocations reported in this study were visually observed for the Eshelby  
5 twist. Eshelby twist was observed in a 1.5 nm × 1.5 nm or larger area around mixed-type  
6 dislocation cores, depending on the mixed-type core structure observed. This large displacement  
7 of atomic columns was used to distinguish between mixed-type and edge-type dislocations in  
8 this study, and in similar previous studies on doped and alloyed GaN<sup>9-11</sup>. The composition  
9 around the dislocations was investigated by energy dispersive X-ray spectroscopy (EDX) in the  
10 FEI Titan G2 80-200 ChemiSTEM microscope. The EDX quantification was based on line scans  
11 taken across the dislocation cores, with a *ca.* 1 nm analysis width, and was performed using a  
12 standard background subtraction and the Cliff-Lorimer factor method. For statistical validity,  
13 over 40 dislocations were observed for core structure identification, and 12 for compositional  
14 analysis.

15  
16  
17  
18  
19  
20  
21  
22  
23  
24  
25  
26  
27  
28  
29  
30  
31  
32 The optical properties of dislocations in AlGa<sub>N</sub> and InGa<sub>N</sub> were compared using a "multi-  
33 microscopy" methodology. As described in Ref. 27, a copper grid for TEM sample preparation  
34 was positioned on the surface of the sample using epoxy resin. Using the 50 μm size square  
35 mesh of the grid, the same set of dislocations could be examined by atomic force microscopy  
36 (AFM) and scanning electron microscopy with cathodoluminescence (SEM-CL). AFM was  
37 conducted on a Veeco Dimension 3100 operating in tapping mode and was used to measure the  
38 size of pits at the termination of dislocations, which allows one to obtain the dislocation type,  
39 and the distance to nearest neighbor, following the procedure described in earlier work<sup>23</sup>. It  
40 should be noted that in the case of the AlGa<sub>N</sub> layer, the dislocations emerging at the surface of  
41 the sample are significantly smaller than the V-shaped pits present in InGa<sub>N</sub>, hence the pit size  
42 was obtained in this sample using the pit depth, instead of the pit width. SEM-CL was conducted  
43  
44  
45  
46  
47  
48  
49  
50  
51  
52  
53  
54  
55  
56  
57  
58  
59  
60

1  
2  
3 at liquid He (10 K) temperature in an Attolight Rosa 4634 CL microscope for the AlGa<sub>N</sub> sample  
4  
5 and a FEI XL30 microscope equipped with a Gatan Mono CL4 CL system for the InGa<sub>N</sub>  
6  
7 sample. The AlGa<sub>N</sub> and InGa<sub>N</sub> samples exhibited a CL peak emission wavelength at 279 nm  
8  
9 (recorded over the 210-345 nm range) and 398 nm (recorded over the 360-425 nm range),  
10  
11 respectively. The SEMs were operated at 3 kV, resulting in the majority of the CL signal  
12  
13 collected arising from the first 25-30 nm of material below the surface. This value was confirmed  
14  
15 using Monte Carlo simulations<sup>28</sup>, taking into account the absorption coefficient of the  
16  
17 materials<sup>29</sup>. SEM-CL was used to analyze the variation in CL intensity and emission energy at  
18  
19 and around the dislocations. This study was conducted at liquid He temperature (10 K) as it  
20  
21 significantly increases the intensity of the CL signal, hence allowing the recording of spectral  
22  
23 maps with a high spectral resolution, here of the order of 1-2 meV.  
24  
25  
26  
27  
28  
29  
30  
31  
32  
33  
34  
35  
36  
37  
38  
39  
40  
41  
42  
43  
44  
45  
46  
47  
48  
49  
50  
51  
52  
53  
54  
55  
56  
57  
58  
59  
60

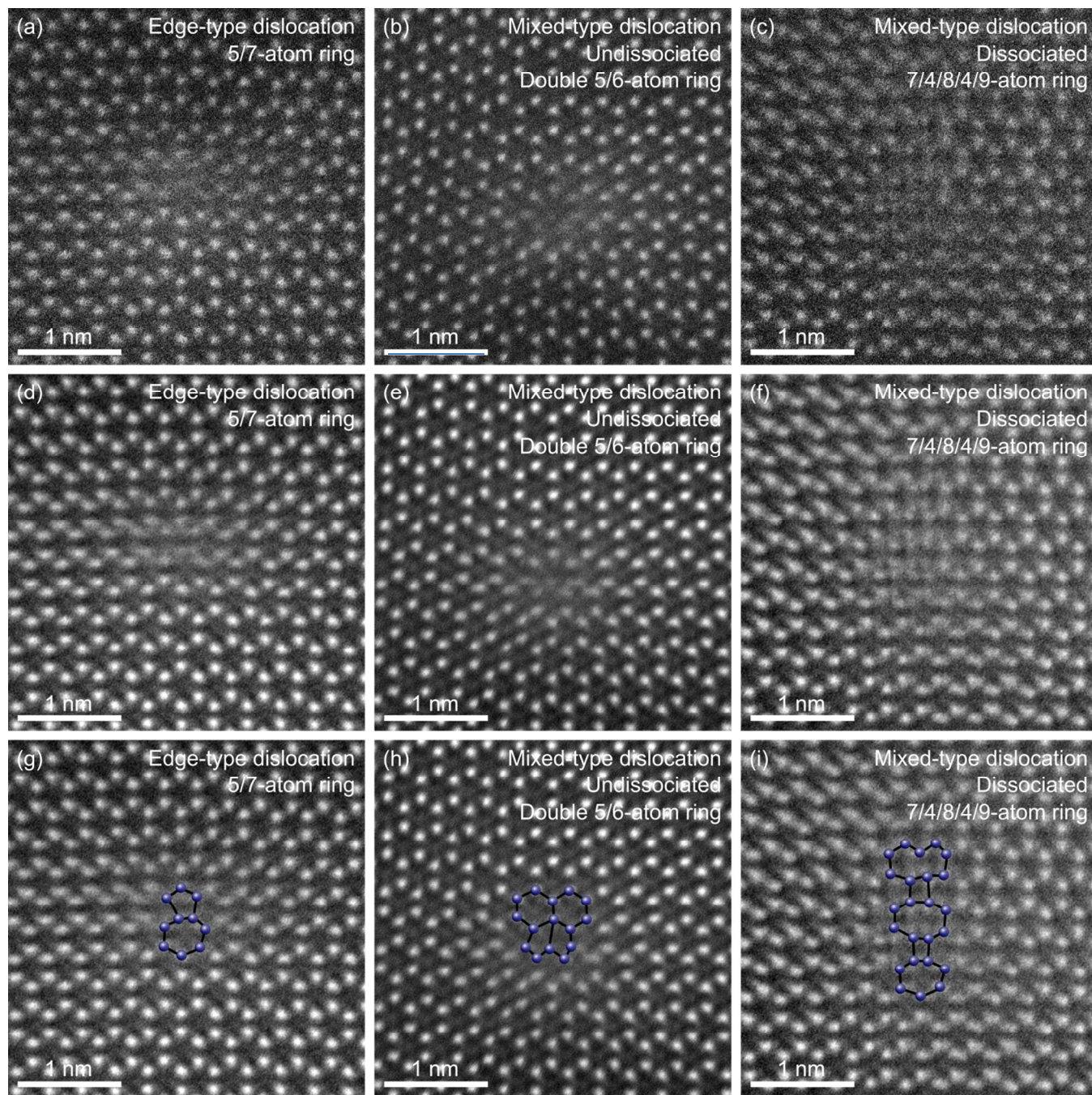


**Figure 1.** Plan-view aberration-corrected HAADF-STEM image of the AlGaIn sample, showing the core structure of an edge-type dislocation (5/7-atom ring)(a,d,g), an undissociated mixed-type dislocation (double 5/6-atom ring)(b,e,h) and a dissociated mixed-type dislocation (7/4/8/4/9-

1  
2  
3 atom ring)(c,f,i). Raw unfiltered images (a-c), and ABSF-filtered (average background  
4 subtraction filter) (d-f) with atomic columns identified to guide the eye (g-i).  
5  
6  
7  
8  
9

10  
11 The core structure of the dislocations in the AlGa<sub>N</sub> sample has been observed by plan-view  
12 aberration corrected HAADF-STEM, and three representative examples are shown in Figure 1.  
13 Akin to other studies performed on GaN<sup>9,10</sup> and InGa<sub>N</sub><sup>11,23</sup>, we observed that 100% of the edge-  
14 type dislocations form 5/7-atom ring cores, as illustrated in Figure 1(g). In the context of mixed-  
15 type dislocations, we observed essentially two different configurations, *i.e.* dissociated and  
16 undissociated core structures. In line with previous reports we observed that the undissociated  
17 core of mixed-type dislocations form a double 5/6-atom ring (Figure 1(h))<sup>9,12</sup>. (The undissociated  
18 core structure shown could either be an 8-atom or a double 5/6-atom ring. A sub-nm spatial  
19 resolution would be required to distinguish between the two configurations. However the energy  
20 of the double 5/6-atom configuration was calculated to be lower than that for 8-atom ring in GaN  
21 films<sup>15</sup>, so it is likely that the core structure in Figure 1(h) is a double 5/6-atom ring.) The  
22 dissociated cores correspond to two partial dislocations with Burgers vector  $\mathbf{b} = 1/2(\mathbf{a}+\mathbf{c}) =$   
23  $1/6[1-213]$  connected by a stacking fault with a displacement vector  $\mathbf{R} = 1/6[1-213]$ , which  
24 results in an elongated core as illustrated by Figure 1(i)<sup>9,12</sup>. The length of the core, that is,  
25 essentially the number of 4/8 rings in the core, can vary from dislocation to dislocation. In this  
26 sample, cores forming 7/4/9, 7/4/8/5, 7/4/8/4/9, and 7/4/8/4/8/5 atom rings have been observed.  
27  
28  
29  
30  
31  
32  
33  
34  
35  
36  
37  
38  
39  
40  
41  
42  
43  
44  
45  
46  
47  
48  
49  
50  
51  
52  
53  
54  
55  
56  
57  
58  
59  
60

**Table 1.** Summary of the proportion of dislocation core configurations for a variety of III-Nitride alloys. LDD stands for low dislocation density (*i.e.*  $\sim 3 \times 10^8 \text{ cm}^{-2}$ ) and HDD stands for high dislocation density (*i.e.*  $\sim 6 \times 10^9 \text{ cm}^{-2}$ ).

Alloy	Doping	TD density	Edge 5/7 atom ring	Mixed Undissociated	Mixed Dissociated	Ref.
GaN	Undoped	LDD	100 %	$50 \pm 5 \%$	$50 \pm 5 \%$	9
GaN	Undoped	HDD	100 %	$50 \pm 5 \%$	$50 \pm 5 \%$	9
GaN	Mg	HDD	100 %	$85 \pm 3\%$	$15 \pm 3 \%$	9
GaN	Si	LDD	100 %	$48 \pm 9 \%$	$54 \pm 9 \%$	10
GaN	Si	HDD	100 %	$57 \pm 3 \%$	$43 \pm 3 \%$	10
$\text{In}_{0.06}\text{Ga}_{0.94}\text{N}$	Si	LDD	100 %	$46 \pm 5 \%$	$54 \pm 5 \%$	11
$\text{In}_{0.20}\text{Ga}_{0.80}\text{N}$	Si	LDD	100 %	$43 \pm 6 \%$	$57 \pm 6 \%$	11
$\text{Al}_{0.46}\text{Ga}_{0.54}\text{N}$	Undoped		100 %	$68 \pm 9 \%$	$32 \pm 9 \%$	This work

Table 1 summarizes the data obtained from this experiment and compares them with results available in the literature for a range of III-Nitride alloys. It appears clearly that the dislocation core structures in AlGaN are consistent with those in other nitride alloys under various conditions of composition, dopant type, or dislocation density. The main notable difference lies in the ratio of dissociated to undissociated mixed-type dislocations, which relates to the elastic strain energy around the dislocation core, and has been used in the past to hint at the segregation of solute species around the dislocation<sup>9</sup>. (We note that In atoms were shown to segregate at dislocations in InGaN despite not exhibiting a meaningful change in the ratio of dissociated to undissociated mixed-type dislocations<sup>11</sup>. This is perhaps because these samples were Si-doped,

1  
2  
3 and that Si segregation at dislocations inhibits dislocation climb, as was reported in GaN<sup>10</sup>.) In  
4  
5 our AlGa<sub>N</sub> sample we can see that the proportion of mixed-type dislocations that dissociate  
6  
7 deviates from the case of undoped GaN, which indicates that alloying with AlN impedes  
8  
9 dislocation dissociation. This is in line with Chen *et al.*, who used first principle density  
10  
11 functional theory calculations to estimate the stability of stacking faults in Mg- and Al-doped  
12  
13 GaN over the entire compositional range, and predicted that, at comparable composition, Al  
14  
15 around threading dislocations would hinder dislocation dissociation, but to a much lesser extent  
16  
17 than Mg<sup>30</sup>. However, Table 1 compares Al and Mg compositions which are several orders of  
18  
19 magnitude different - 46% and << 0.1% for Al and Mg respectively. Therefore the results from  
20  
21 this theoretical work are not directly transferrable to our study, yet it is worth pointing out that  
22  
23 Table 1 shows that Mg-doped GaN exhibits the lowest proportion of dislocation dissociation,  
24  
25 followed by AlGa<sub>N</sub>. A lower proportion of dislocation dissociation can be attributed to virtually  
26  
27 any factor that may affect the energies involved in the formation of a dissociated core, that is, the  
28  
29 elastic strain energy of the dislocation, the stacking fault energy, or the dislocation core energy.  
30  
31 Given that dislocations in AlGa<sub>N</sub> do not seem to differ from other III-Nitrides alloys - as far as  
32  
33 the core structure is concerned - and that Mg and In have been previously found to segregate  
34  
35 around the dislocations, consequently reducing the elastic strain energy<sup>9,11,23,31</sup>, it is appropriate  
36  
37 to investigate whether similar non-uniformities are seen in the distribution of Al and Ga atoms in  
38  
39 the vicinity of dislocations in AlGa<sub>N</sub>.  
40  
41  
42  
43  
44  
45  
46  
47  
48  
49  
50  
51  
52  
53  
54  
55  
56  
57  
58  
59  
60

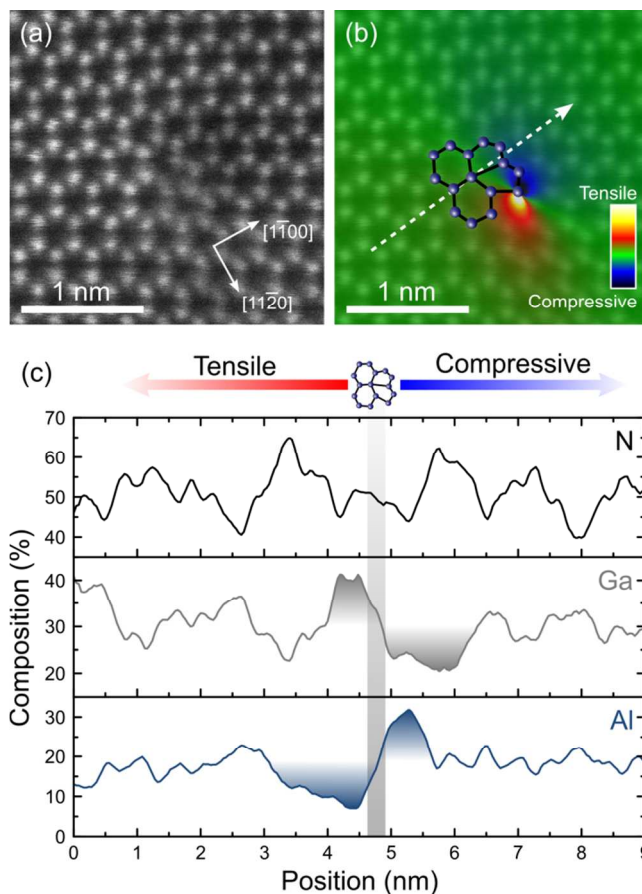


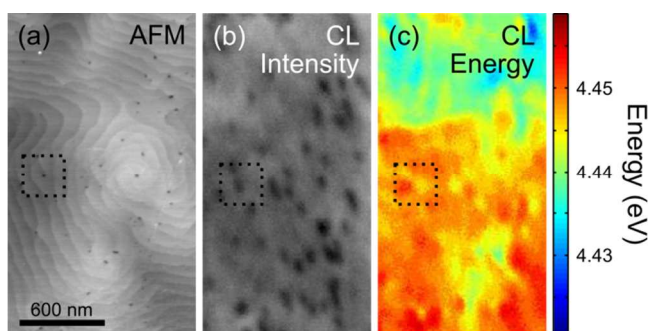
**Figure 2.** (a) Unfiltered HAADF-STEM image of an undissociated mixed-type dislocation. (b) ABSF-filtered image of (a) with geometric phase analysis overlay showing the x-x strain component (x-axis parallel to [11-20]). (c) EDX line scan showing the composition of Al, Ga, and N along the line depicted in (b) (with a *ca.* 1 nm analysis width).

EDX mapping of dislocations has been conducted inside the TEM. This enabled us to investigate potential connections between the dislocation type and core configuration (obtained through the HAADF-STEM images) to the strain distribution around the dislocation (obtained through geometric phase analysis of the HAADF-STEM images) and to the distribution of Al and Ga atoms around the dislocation (obtained through the EDX map). This is illustrated in

1  
2  
3  
4  
5  
6  
7  
8  
9  
10  
11  
12  
13  
14  
15  
16  
17  
18  
19  
20  
21  
22  
23  
24  
25  
26  
27  
28  
29  
30  
31  
32  
33  
34  
35  
36  
37  
38  
39  
40  
41  
42  
43  
44  
45  
46  
47  
48  
49  
50  
51  
52  
53  
54  
55  
56  
57  
58  
59  
60

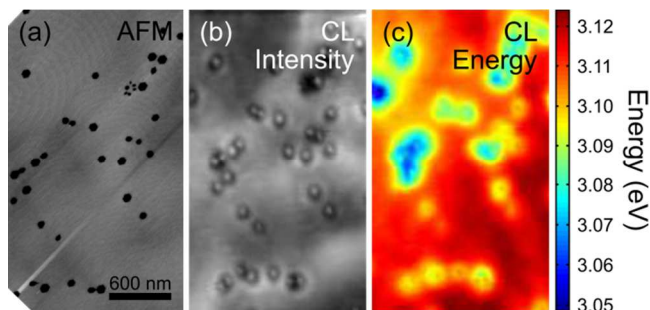
Figure 2 for an undissociated mixed-type dislocation. The geometric phase analysis overlay (here used qualitatively only) shows that the dislocation core is bounded on either side by a region of compressive strain and a region of tensile strain, as expected by the elasticity theory of dislocations. (We also note an asymmetry of the geometric phase analysis map, presumably ascribable to Eshelby twist<sup>26</sup>). An EDX line scan taken across the dislocation core and from the tensile side to the compressive side, as illustrated in Figure 2(b), reveals the compositional fluctuations around the dislocation. It can be seen in Figure 2(c) that the dislocation core is bounded by a Ga-rich (or Al-poor) region and an Al-rich (or Ga-poor) region (this is particularly noticeable on the Al trace). The segregation of species occurs in close vicinity of the core, on a length scale of about 1-2 nm. The region of higher Ga content is found to relate to the side of the dislocation under tensile strain, whilst the region of higher Al content relates to the side under compressive strain. This is explained by the Al-N bond being shorter than the Ga-N bond<sup>32</sup> (in a relaxed  $\text{Al}_{0.5}\text{Ga}_{0.5}\text{N}$  alloy, valence force field simulations predicted the Al-N bond to be about 2% shorter than Ga-N), which leads to a reduction of the elastic strain around the dislocation if Ga and Al segregate at the tensile and compressive side of the dislocation, respectively. Our experimental observation agrees with Sakaguchi *et al.* who used empirical interatomic potentials and Monte Carlo simulations to study alloy segregation at dislocations in  $\text{Al}_{0.3}\text{Ga}_{0.7}\text{N}$ , and found that Ga and Al atoms segregate in the tensile and compressive part, respectively, of dislocations with an edge component<sup>33</sup>. We observed similar results irrespectively of the dislocation core configuration, *i.e.* edge, mixed undissociated, mixed dissociated (no screw dislocations were investigated here). This result is consistent with our earlier finding that mixed-type dislocations in AlGa<sub>3</sub>N do not dissociate to as great an extent as in GaN. The segregation of Al and Ga atoms reduces the elastic strain of the dislocation, therefore reducing the driving force for dissociation.

1  
2  
3 The phenomenon of atom segregation at dislocations has also been reported in InGaN  
4 alloys<sup>11,31</sup> and has been shown to affect the carrier recombination at the dislocation<sup>23</sup>. In the case  
5 of InGaN, we have suggested that the segregation of In atoms promotes the formation of In-N-In  
6 chains and atomic condensates in the tensile part of the dislocation core, which strongly localizes  
7 holes<sup>34-36</sup>, and consequently limits non-radiative recombination at the dislocation core. Since  
8 dislocations in AlGaN are surrounded by an Al-rich region and a Ga-rich region, it is sensible to  
9 consider the possibility that these may alter the carrier recombination in the vicinity of the  
10 dislocation.  
11  
12  
13  
14  
15  
16  
17  
18  
19  
20  
21  
22  
23



36  
37  
38  
39  
40  
41  
42

**Figure 3.** (a) AFM, (b) CL integrated intensity, and (c) CL peak emission energy of the same region in the AlGaN sample.



54  
55  
56  
57  
58  
59  
60

**Figure 4.** (a) AFM, (b) CL integrated intensity, and (c) CL peak emission energy of the same region in the InGaN sample.

1  
2  
3 In order to investigate whether the segregation of species reported above has any effect on the  
4 optical properties of the dislocations, a multi-microscopy approach based on the combined  
5 analysis of AFM, SEM and CL data recorded at liquid He temperatures, has been employed on  
6 the AlGa<sub>N</sub> sample and is illustrated in Figure 3. For comparison, the same approach under  
7 similar experimental conditions has been employed on the InGa<sub>N</sub> sample and is presented in  
8 Figure 4. The dislocations are readily observable by AFM as they appear at the surface of the  
9 sample, as small pits in AlGa<sub>N</sub> (Figure 3(a)), and as larger V-shaped pits in InGa<sub>N</sub> (Figure 4(a)).  
10 A one-to-one correlation can be found between the dislocations identified in the AFM and the  
11 dark spots observed on the CL intensity map (Figure 3(b)), which highlights the non-radiative  
12 behavior of the dislocations in AlGa<sub>N</sub>. This result, although in agreement with the classical  
13 picture of dislocations in semiconductors, including GaN<sup>37-39</sup>, deviates strongly with what can be  
14 observed in InGa<sub>N</sub>. As can be seen in Figure 4(b), the dislocations in InGa<sub>N</sub> appear in the CL  
15 intensity image as a bright spot surrounded by a dark halo. In our earlier work, this bright spot  
16 has been linked to the carrier localization deriving from the segregation of In atoms at the  
17 dislocation<sup>23</sup>. Previous studies investigating carrier dynamics in thick AlGa<sub>N</sub> epilayers reported  
18 that excitons were localized at low temperature at compositional fluctuations in the alloy<sup>40-42</sup>.  
19 The CL data presented in Figure 3(b) suggest that if carriers are localized in the vicinity of the  
20 dislocations due to the atom segregation, the effect on the CL emission intensity is very limited  
21 in contrast to what is observed in InGa<sub>N</sub>. This corroborates experimental<sup>34</sup> and theoretical<sup>35</sup>  
22 studies which showed that carrier localization induced by In atoms is much stronger than carrier  
23 localization from Ga or Al atoms. This result may provide an explanation for the relative  
24 resilience of InGa<sub>N</sub>-based devices to dislocations, as opposed to AlGa<sub>N</sub>-based. We could thus  
25 hypothesize that doping AlGa<sub>N</sub> with In may be an interesting way to enhance radiative  
26  
27  
28  
29  
30  
31  
32  
33  
34  
35  
36  
37  
38  
39  
40  
41  
42  
43  
44  
45  
46  
47  
48  
49  
50  
51  
52  
53  
54  
55  
56  
57  
58  
59  
60

1  
2  
3 recombination at dislocations, as the In atoms may segregate in the tensile part of the  
4 dislocations and (strongly) localize carriers.  
5  
6

7  
8 The CL peak emission energy map for the two alloys is presented in Figures 3(c) and 4(c). As  
9 reported previously in InGaN, the emission energy corresponding to the bright spot is redshifted  
10 compared to that of the surrounding material far away from the dislocation, in agreement with  
11 the presence of In-N-In chains and atomic condensates localizing carriers at the dislocation<sup>23</sup>.  
12  
13 Conversely, in AlGaN, the dislocations are bounded on either side by a redshifted and a  
14 blueshifted region, as illustrated by the dislocation inside the dotted square in Figure 3. For  
15 dislocations which are isolated, that is, typically more than 150 nm away from the nearest  
16 neighbouring dislocation, the energy shifts of these regions relative to the emission energy at the  
17 dislocation position is very symmetric, with values of  $-4 \pm 2$  meV and  $3 \pm 2$  meV for the  
18 redshifted and blueshifted part, respectively, with no measurable difference based on the  
19 dislocation type. (For dislocations with distance to nearest neighbor below 150 nm, the  
20 redshifted and blueshifted regions of both dislocations tend to overlap, making data analysis less  
21 reliable in that case.) This dipole-like energy shift seems to indicate that the energy shifts may be  
22 ascribed to the strain distribution around the dislocation.  
23  
24  
25  
26  
27  
28  
29  
30  
31  
32  
33  
34  
35  
36  
37  
38  
39  
40  
41  
42  
43  
44  
45  
46  
47  
48  
49  
50  
51  
52  
53  
54  
55  
56  
57  
58  
59  
60

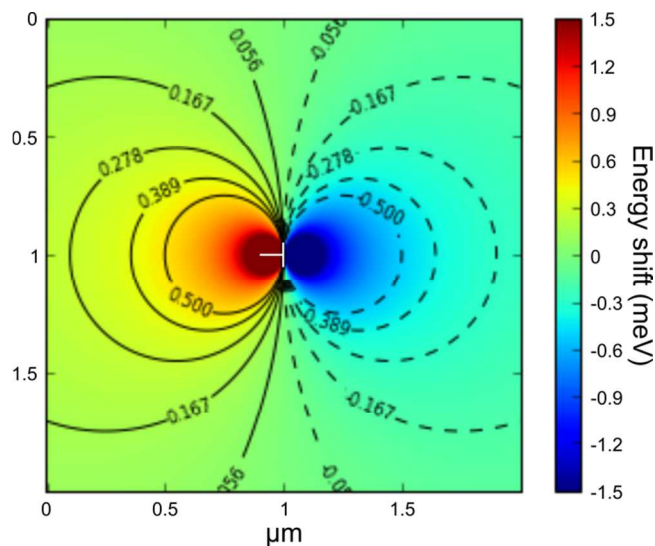


**Figure 5.** Simulation of the emission energy shift in the vicinity of an edge-type dislocation.

To further investigate the origin of the energy shift reported above, we conducted continuum elastic calculations to describe the strain field and emission energy shifts around an edge-type dislocation. This approach has been well-described by Gmeinwieser *et al.* to study dislocations in GaN<sup>43</sup>. We thus adopted a similar approach here, for our Al<sub>0.46</sub>Ga<sub>0.54</sub>N sample, using the elastic constants from Ref. 44 and deformation potentials from Ref. 45 for GaN and AlN, and assuming Vegard's law applies. These calculations considered a random alloy of Al<sub>0.46</sub>Ga<sub>0.54</sub>N, that is, with no segregation in the vicinity of the dislocations. The results of the simulation are presented in Figure 5, where a shift of typically -1.5 meV and 1.5 meV are predicted for the tensile and compressive parts, respectively. These values are of the same order as the experimental values of  $-4 \pm 2$  meV and  $3 \pm 2$  meV we reported. The simulations seem nevertheless to underestimate slightly the value of the emission energy shift, presumably indicating some effect of alloy segregation on the emission energy shift - *i.e.* the segregation of Ga atoms in the tensile part of the dislocation increases the (negative) energy shift, while the segregation of Al in the compressive part increases the (positive) energy shift.

1  
2  
3 In conclusion we conducted a comprehensive investigation of dislocations in AlGa<sub>N</sub> material  
4 with an Al content ~ 46%. The core configuration of the dislocations has been identified. We  
5  
6 thus report that the dislocation core structure is in line with that of other III-Nitride alloys, but  
7  
8 that alloying GaN with AlN tends to prevent the dissociation of mixed-type dislocations. We  
9  
10 show that this is due to Ga and Al atoms segregation in the tensile and compressive parts of the  
11  
12 dislocation, respectively. Finally, we investigated the optical implications of these alloy  
13  
14 segregations. Unlike in InGa<sub>N</sub> alloys, where In atom segregation at dislocation also occurs, the  
15  
16 segregation of Al and Ga atoms does not significantly affect the optical properties of dislocations  
17  
18 in AlGa<sub>N</sub>. This study gives insights on why InGa<sub>N</sub>-based devices are generally more resilient to  
19  
20 dislocations than their AlGa<sub>N</sub>-based counterparts, and brings forwards the hypothesis that  
21  
22 doping AlGa<sub>N</sub> with In may be an interesting approach to hinder non-radiative recombination at  
23  
24 dislocations.  
25  
26  
27  
28  
29  
30  
31  
32  
33

#### 34 AUTHOR INFORMATION

##### 36 **Corresponding Author**

37  
38  
39 \* E-mail: fm350@cam.ac.uk  
40  
41

##### 42 **Author Contributions**

43  
44  
45 The manuscript was written through contributions of all authors. All authors have given approval  
46  
47 to the final version of the manuscript.  
48  
49

##### 50 **Notes**

51  
52  
53 The authors declare no competing interest.  
54  
55  
56  
57  
58  
59  
60

## Funding Sources

European Research Council, European Union Seventh Framework Programme, Lindemann Trust.

## ACKNOWLEDGMENT

This project is funded in part by the European Research Council under the European Community's Seventh Framework Programme (FP7/2007-2013)/ERC grant agreement No. 279361 (MACONS). The research leading to these results has received funding from the European Union Seventh Framework Programme under Grant Agreement 312483 - ESTEEM2 (Integrated Infrastructure Initiative I3). S.R. acknowledges financial support from the ERC Starting Grant 307636 "SCOPE". M.H. would like to acknowledge support from the Lindemann Trust Fellowship. Datasets for the figures in this paper can be found at <https://doi.org/10.17863/CAM.10364>.

## ABBREVIATIONS

LED, light emitting diode; UV, ultra-violet; MOVPE, metal-organic vapor phase epitaxy; TMG, trimethylgallium; TMA, trimethylaluminium; TMI, trimethylindium; SiH<sub>4</sub>, silane; NH<sub>3</sub>, ammonia; H<sub>2</sub>, hydrogen; N<sub>2</sub>, nitrogen; HAADF-STEM, high-angle annular dark field scanning transmission electron microscopy; EDX, energy dispersive X-ray spectroscopy; AFM, atomic force microscopy; SEM, scanning electron microscopy; CL, cathodoluminescence; LDD, low dislocation density; HDD, high dislocation density.

## REFERENCES

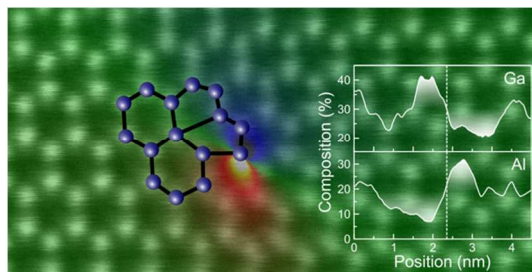
- (1) Nakamura, S. *Ann. Phys. (Berlin)* **2015**, 527, 335-349.
- (2) Humphreys, C.J. *MRS Bulletin* **2008**, 33, 459-470.

- 1  
2  
3 (3) Kneissl, M.; Rass, J. *III-Nitride Ultraviolet Emitters*; Springer: Switzerland, 2016.  
4  
5  
6 (4) Narukawa, Y.; Ichikawa, M.; Sanga, D.; Sano, M.; Mukai, T. *J. Phys. D: Appl. Phys.* **2010**,  
7  
8  
9 43, 354002.  
10  
11 (5) Alhassan, A.I.; Farrell, R.M.; Saifaddin, B.; Mughal, A.; Wu, F.; Denbaars, S.P.;  
12  
13 Nakamura, S.; Speck, J.S. *Opt. Express* **2016**, 24, 17868.  
14  
15  
16 (6) Davies, M.J.; Dawson, P.; Massabuau, F.C.-P.; Oehler, F.; Oliver, R.A.; Kappers, M.J.;  
17  
18  
19 Badcock, T.J.; Humphreys, C.J. *Phys. Status Solidi C* **2014**, 11, 750-753.  
20  
21  
22 (7) Kneissl, M.; Kolbe, T.; Chua, C.; Kueller, V.; Lobo, N.; Stellmach, J.; Knauer, A.;  
23  
24  
25 Rodriguez, H.; Einfeldt, S.; Yang, Z.; Johnson, N.M.; Weyers, M. *Semicond. Sci. Technol.* **2011**,  
26  
27  
28 26, 014036.  
29  
30 (8) Narayanan, V.; Lorenz, K.; Kim, W.; Mahajan, S. *Phil. Mag. A* **2002**, 82, 885-912.  
31  
32  
33 (9) Rhode, S.; Horton, M.; Kappers, M.; Zhang, S.; Humphreys, C.; Dusane, R.; Sahonta, S.-  
34  
35  
36 L.; Moram, M. *Phys. Rev. Lett.* **2013**, 111, 025502.  
37  
38  
39 (10) Rhode, S.L.; Horton, M.K.; Fu, W.Y.; Sahonta, S.-L.; Kappers, M.J.; Pennycook, T.J.;  
40  
41  
42 Humphreys, C.J.; Dusane, R.O.; Moram, M.A. *Appl. Phys. Lett.* **2015**, 107, 243104.  
43  
44  
45 (11) Rhode, S.L.; Horton, M.K.; Sahonta, S.-L.; Kappers, M.J.; Haigh, S.J.; Pennycook, T.J.;  
46  
47  
48 McAleese, C.; Humphreys, C.J.; Dusane, R.O.; Moram, M.A. *J. Appl. Phys.* **2016**, 119, 105301.  
49  
50  
51 (12) Hirsch, P.B.; Lozano, J.G.; Rhode, S.; Horton, M.K.; Moram, M.A.; Zhang, S.; Kappers,  
52  
53  
54 M.J.; Humphreys, C.J.; Yasuhara, A.; Okunishi, E.; Nellist, P.D. *Phil. Mag.* **2013**, 93, 3925-  
55  
56  
57 3938.  
58  
59  
60

- 1  
2  
3 (13) Yang, H.; Lozano, J.G.; Pennycook, T.J.; Jones, L.; Hirsch, P.B.; Nellist, P.D. *Nat. Com.*  
4  
5 **2015**, *6*, 7266.  
6  
7  
8  
9 (14) Arslan, I.; Bleloch, A.; Stach, E.A.; Browning, N.D. *Phys. Rev. Lett.* **2005**, *94*, 025504.  
10  
11  
12 (15) Horton, M.K.; Rhode, S.L.; Moram, M.A. *J. Appl. Phys.* **2014**, *116*, 063710.  
13  
14  
15 (16) Blumenau, A.T.; Elsner, J.; Jones, R.; Heggie, M.I.; Oberg, S.; Frauenheim, T.; Briddon,  
16  
17 P.R. *J. Phys.: Condens. Matter* **2000**, *12*, 10223-10233.  
18  
19  
20 (17) Béré, A.; Serra, A. *Phys. Rev. B* **2002**, *65*, 205323.  
21  
22  
23 (18) Lee, S.M.; Belkhir, M.A.; Zhu, X.Y.; Lee, Y.H.; Hwang, Y.G.; Frauenheim, T. *Phys. Rev.*  
24  
25 *B* **2000**, *61*, 16033-16039.  
26  
27  
28 (19) Belabbas, I.; Béré, A.; Chen, J.; Petit, S.; Akli Belkhir, M.; Ruterana, P.; Nouet, G. *Phys.*  
29  
30 *Rev. B* **2007**, *75*, 115201.  
31  
32  
33 (20) Belabbas, I.; Chen, J.; Nouet, G. *Computational Materials Science* **2014**, *90*, 71-81.  
34  
35  
36 (21) Chen, J.; Ruterana, P.; Nouet, G. *Materials Science and Engineering* **2001**, *B82*, 117-119.  
37  
38  
39 (22) Sridhara Rao, D.V.; Kappers, M.J.; McAleese, C.; Zhu, T.; Zhu, D.; Humphreys, C.J.  
40  
41 "Microstructural study of AlGa<sub>N</sub>/Al<sub>N</sub> buffer with 3D Ga<sub>N</sub> interlayer", *XV International*  
42  
43 *Workshop on Physics of Semiconductor Devices (IWPSD)* **2009**, 264-267.  
44  
45  
46 (23) Massabuau, F.C-P.; Chen, P.; Horton, M.K.; Rhode, S.L.; Ren, C.X.; O'Hanlon, T.J.;  
47  
48 Kovács, A.; Kappers, M.J.; Humphreys, C.J.; Dunin-Borkowski, R.E.; Oliver, R.A. *J. Appl.*  
49  
50 *Phys.* **2017**, *121*, 013104.  
51  
52  
53  
54  
55  
56  
57  
58  
59  
60

- 1  
2  
3 (24) Ernst Ruska-Centre for Microscopy and Spectroscopy with Electrons. *Journal of large-*  
4 *scale research facilities* **2016**, *2*, A43. <http://dx.doi.org/10.17815/jlsrf-2-68>.  
5  
6  
7  
8  
9 (25) Ernst Ruska-Centre for Microscopy and Spectroscopy with Electrons (ER-C). *Journal of*  
10 *large-scale research facilities*, **2015**, *1*, A34. <http://dx.doi.org/10.17815/jlsrf-1-57>.  
11  
12  
13  
14 (26) Lozano, J.G.; Yang, H.; Guerrero-Lebrero, M.P.; D'Alfonso, A.J.; Yasuhara, A.;  
15 Okunishi, E; Zhang, S.; Humphreys, C.J.; Allen, L.J.; Galindo, P.L.; Hirsch, P.B.; Nellist, P.D.  
16  
17 *Phys. Rev. Lett.* **2014**, *113*, 135503.  
18  
19  
20  
21  
22 (27) Massabuau, F.C.-P.; Trinh-Xuan, L.; Lodie, D.; Thrush, E.J.; Zhu, D.; Oehler, F.; Zhu,  
23 T.; Kappers, M.J.; Humphreys, C.J.; Oliver, R.A. *J. Appl. Phys.* **2013**, *113*, 073505.  
24  
25  
26  
27  
28 (28) Drouin, D.; Hovington, P.; Gauvin, R. *Scanning* **1997**, *19*, 20-28.  
29  
30  
31 (29) Muth, J.F.; Brown, J.D.; Johnson, M.A.L.; Yu, Z.; Kolbas, R.M.; Cook Jr., J.W.;  
32 Schetzina, J.F. *Mat. Res. Soc. Symp. Proc.* **1999**, *537*, G5.2.  
33  
34  
35  
36  
37 (30) Chen, C.; Meng, F.; Song, J. *J. Appl. Phys.* **2016**, *119*, 064302.  
38  
39  
40 (31) Horton, M.K.; Rhode, S.; Sahonta, S.-L.; Kappers, M.J.; Haigh, S.J.; Pennycook, T.J.;  
41 Humphreys, C.J.; Dusane, R.O.; Moram, M.A. *Nano Lett.* **2015**, *15*, 923-930.  
42  
43  
44  
45 (32) Mattila, T.; Zunger, A. *J. Appl. Phys.* **1999**, *85*, 160-167.  
46  
47  
48  
49 (33) Sakaguchi, R.; Akiyama, T.; Nakamura, K.; Ito, T. *Jpn. J. Appl. Phys.* **2016**, *55*, 05FM05.  
50  
51  
52 (34) Chichibu, S.; Uedono, A.; Onuma, T.; Haskell, B.; Chakraborty, A.; Koyama, T.; Fini, P.;  
53 Keller, S.; Denbaars, S.; Speck, J.; Mishra, U.; Nakamura, S.; Yamaguchi, S.; Kamiyama, S.;  
54 Amano, H.; Akasaki, I.; Han, J.; Sota, T. *Nat. Mater.* **2006**, *5*, 810-816.  
55  
56  
57  
58  
59  
60

- 1  
2  
3 (35) Liu, Q.; Lu, J.; Gao, Z.; Lai, L.; Qin, R.; Li, H.; Zhou, J.; Li, G. *Phys. Status Solidi B*  
4  
5 **2010**, *247*, 109-114.  
6  
7  
8  
9 (36) Schulz, S.; Marquardt, O.; Coughlan, C.; Caro, M.A.; Brandt, O.; O'Reilly, E.P. *Proc. of*  
10  
11 *SPIE* **2015**, *9357*, 93570C.  
12  
13  
14 (37) Sugahara, T.; Sato, H.; Hao, M.; Naoi, Y.; Kurai, S.; Tottori, S.; Yamashita, K.; Nishino,  
15  
16 K.; Romano, L.T.; Sakai, S. *Jpn. J. Appl. Phys.* **1998**, *37*, L398-L400.  
17  
18  
19  
20 (38) Cherns, D.; Henley, S.J.; Ponce, F.A. *Appl. Phys. Lett.* **2001**, *78*, 2691-2693.  
21  
22  
23  
24 (39) Rosner, S.J.; Carr, E.C.; Ludowise, M.J.; Girolami, G.; Erikson, H.I. *Appl. Phys. Lett.*  
25  
26 **1997**, *70*, 420-422.  
27  
28  
29 (40) Onuma, T.; Chichibu, S.F.; Uedono, A.; Sota, T.; Cantu, P.; Katona, T.M.; Keading, J.F.;  
30  
31 Keller, S.; Mishra, U.K.; Nakamura, S.; DenBaars, S.P. *J. Appl. Phys.* **2004**, *95*, 2495-2504.  
32  
33  
34 (41) Nepal, N.; Li, J.; Nakarmi, M.L.; Lin, J. Y.; Jiang, H.X. *Appl. Phys. Lett.* **2006**, *88*,  
35  
36 062103.  
37  
38  
39 (42) Rigutti, L.; Mancini, L.; Lefebvre, W.; Houard, J.; Hernández-Maldonado, D.; Di Russo,  
40  
41 E.; Giraud, E.; Butté, R.; Carlin, J.-F.; Grandjean, N.; Blavette, D.; Vurpillot, F. *Semicond. Sci.*  
42  
43 *Technol.* **2016**, *31*, 095009.  
44  
45  
46 (43) Gmeinwieser, N.; Schwarz, U.T. *Phys. Rev. B* **2007**, *75*, 245213.  
47  
48  
49 (44) Vurgaftman, I.; Meyer, J.R. *J. Appl. Phys.* **2003**, *94*, 3675-3696.  
50  
51  
52 (45) Yan, Q.; Rinke, P.; Janotti, A.; Scheffler, M.; Van de Walle, C.G. *Phys. Rev. B* **2014**, *90*,  
53  
54 125118.  
55  
56  
57  
58  
59  
60



1  
2  
3  
4  
5  
6  
7  
8  
9  
10  
11  
12  
13  
14  
15  
16  
17  
18  
19  
20  
21  
22  
23  
24  
25  
26  
27  
28  
29  
30  
31  
32  
33  
34  
35  
36  
37  
38  
39  
40  
41  
42  
43  
44  
45  
46  
47  
48  
49  
50  
51  
52  
53  
54  
55  
56  
57  
58  
59  
60

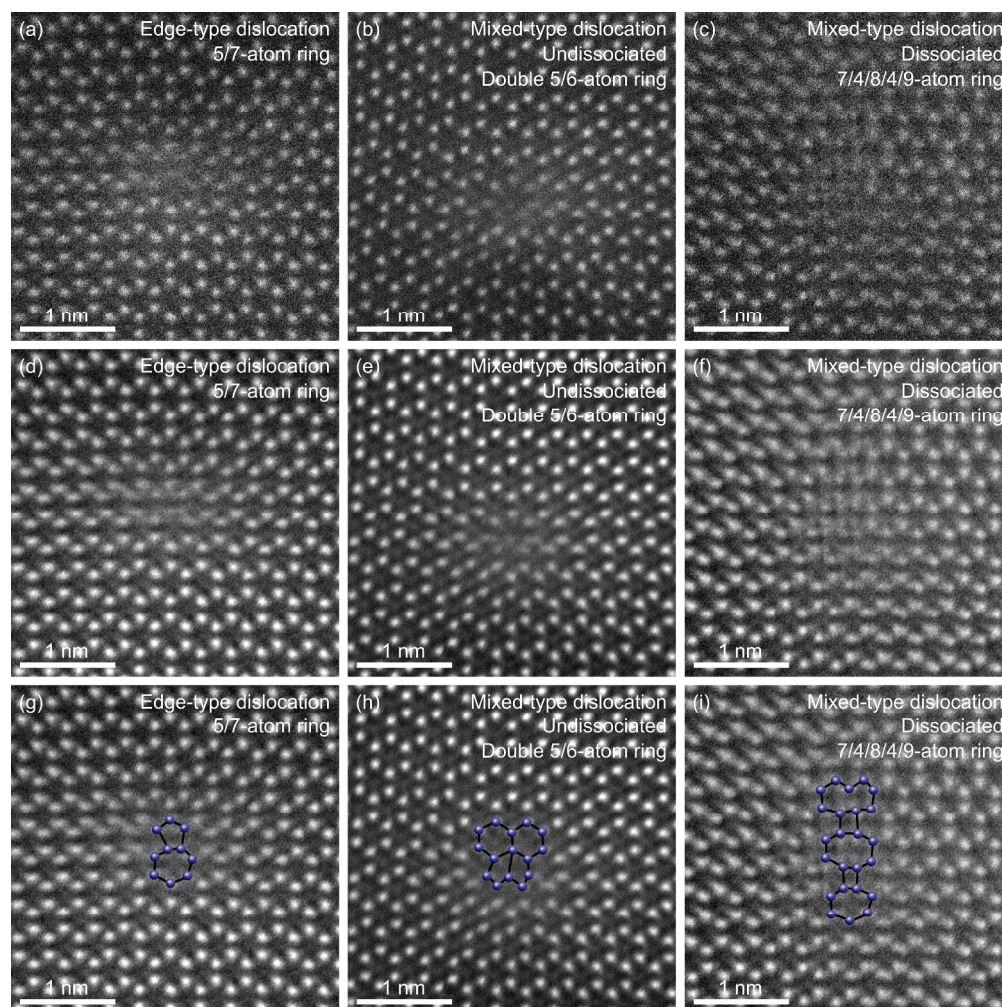


Figure 1. Plan-view aberration-corrected HAADF-STEM image of the AlGaIn sample, showing the core structure of an edge-type dislocation (5/7-atom ring)(a,d,g), an undissociated mixed-type dislocation (double 5/6-atom ring)(b,e,h) and a dissociated mixed-type dislocation (7/4/8/4/9-atom ring)(c,f,i). Raw unfiltered images (a-c), and ABSF-filtered (average background subtraction filter) (d-f) with atomic columns identified to guide the eye (g-i).

1111x1110mm (96 x 96 DPI)

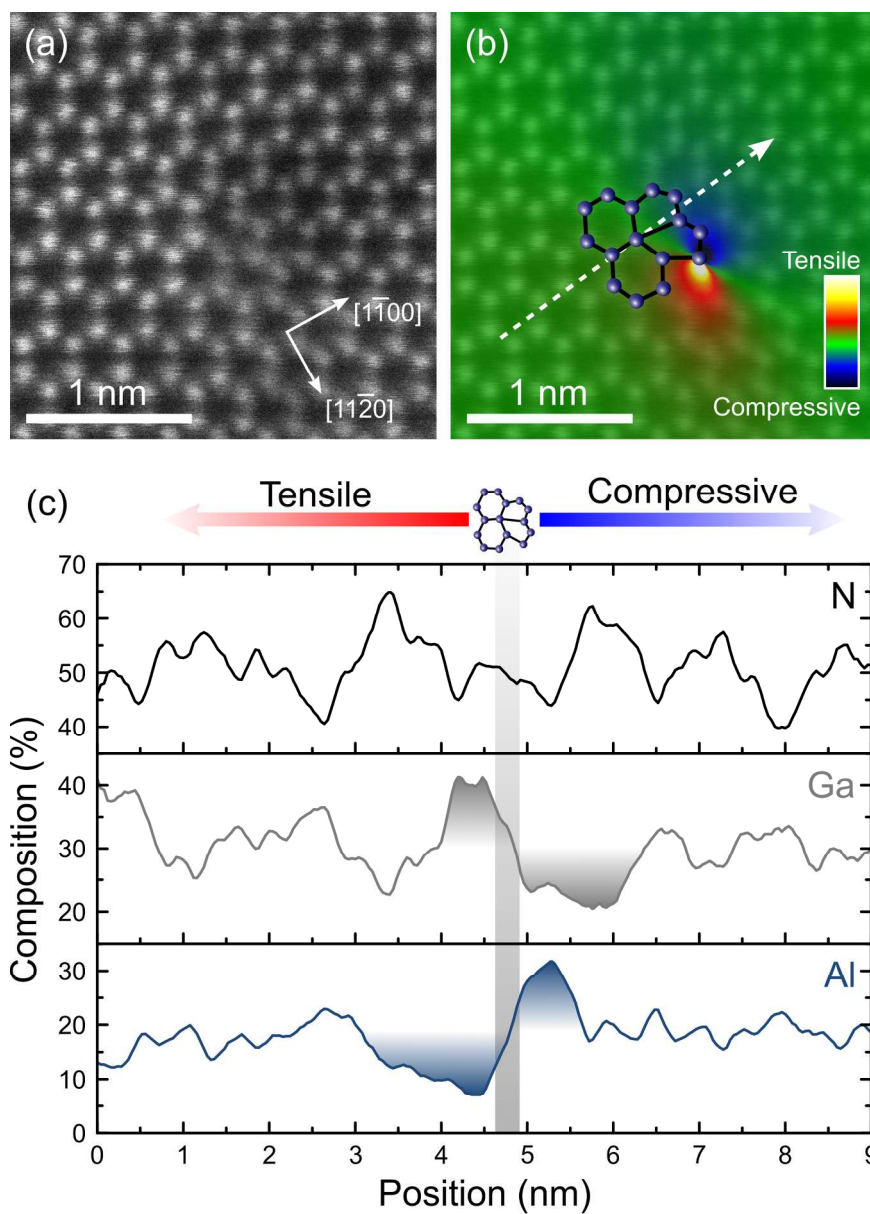


Figure 2. (a) Unfiltered HAADF-STEM image of an undissociated mixed-type dislocation. (b) ABSF-filtered image of (a) with geometric phase analysis overlay showing the x-x strain component (x-axis parallel to  $[11\bar{2}0]$ ). (c) EDX line scan showing the composition of Al, Ga, and N along the line depicted in (b) (with a ca. 1 nm analysis width).

528x731mm (96 x 96 DPI)

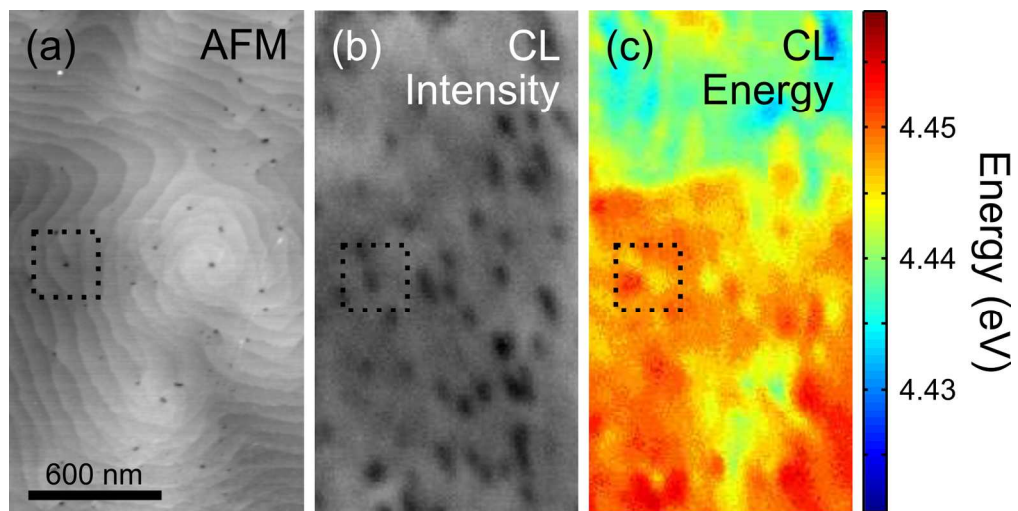


Figure 3. (a) AFM, (b) CL integrated intensity, and (c) CL peak emission energy of the same region in the AlGaIn sample.

528x265mm (96 x 96 DPI)

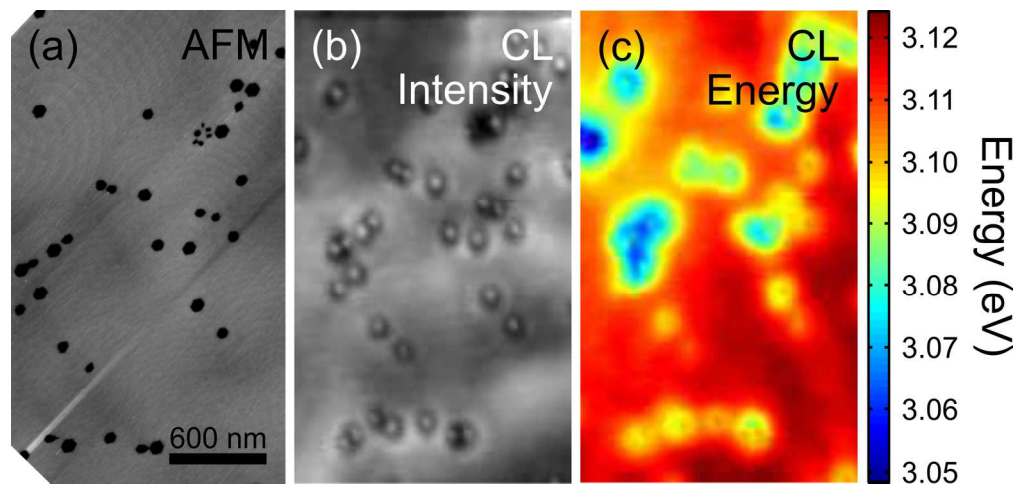


Figure 4. (a) AFM, (b) CL integrated intensity, and (c) CL peak emission energy of the same region in the InGaN sample.

528x250mm (96 x 96 DPI)

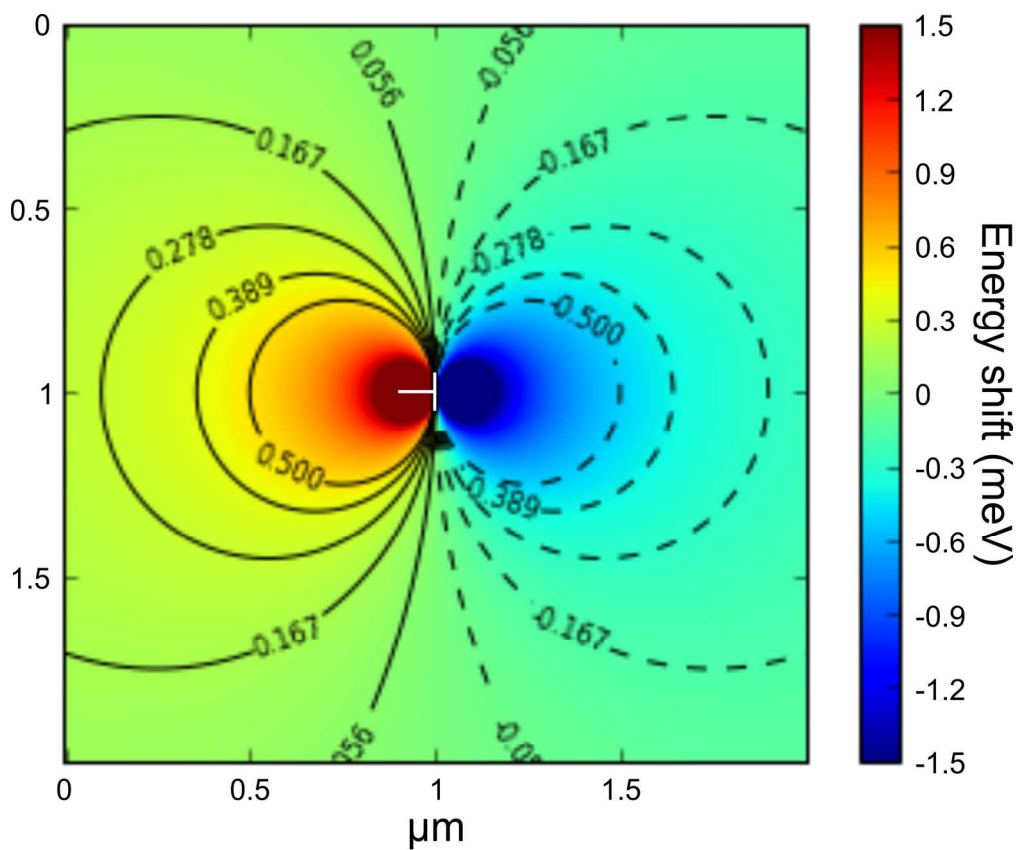


Figure 5. Simulation of the emission energy shift in the vicinity of an edge-type dislocation.

528x441mm (96 x 96 DPI)

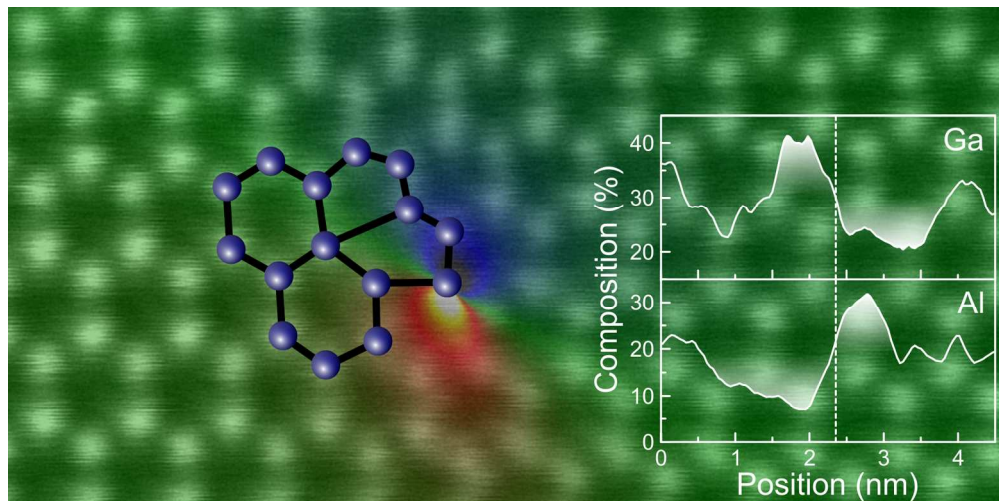


Table of Content Graphic

500x249mm (96 x 96 DPI)